Recent Progress in the Synthesis and Characterization of Amorphous and Crystalline Carbon Nitride Coatings

Ian Widlow and Yip-Wah Chung
Department of Materials Science and Engineering
Northwestern University, Evanston, Illinois 60208, USA

Received 28 January, 2000

This review summarizes our most recent findings in the structure and properties of amorphous and crystalline carbon nitride coatings, synthesized by reactive magnetron sputtering. By careful control of the plasma conditions via proper choice of process parameters such as substrate bias, target power and gas pressure, one can precisely control film structure and properties. With this approach, we were able to produce amorphous carbon nitride films with controlled hardness and surface roughness. In particular, we can synthesize ultrathin (1 nm thick) amorphous carbon nitride films to be sufficiently dense and uniform that they provide adequate corrosion protection for hard disk applications. We demonstrated the strong correlation between ZrN(111) texture and hardness in CN_x/ZrN superlattice coatings. Raman spectroscopy and near-edge x-ray absorption show the predominance of sp^3-bonded carbon in these superlattice coatings.

I Introduction

The desire for greater storage density on computer hard disks continues to propel research around the world. Better magnetic materials and introduction of magneto-resistive read-head technology have provided some of the improvements. However, reducing the magnetic spacing is essential for further improvement in storage density. Defined as the separation between the head and the top of the magnetic media, the magnetic spacing is composed of the pole-tip recession, air bearing, lubricant film, and the protective overcoat. Decreasing the air bearing increases storage density, but also increases the probability of head-disk contact and damage to the underlying magnetic layer. An alternate solution is to make the protective overcoat thinner (currently just a few nm). However, one cannot do this simply by reducing the deposition time. Hardness, scratch resistance, corrosion resistance, and reactivity with the lubricant must all be optimized.

Amorphous carbon nitride (CN_x) is currently the most widely used material in protective overcoats for hard disks. The maximum reported hardness varies between 25 and 35 GPa. In 1989, a prediction was made that β-C_3N_4, a theoretical phase with hexagonal symmetry, would have a bulk modulus approaching that of diamond [1,2]. With hardness roughly scaling to 10 percent of the Young's modulus in hard materials such as diamond (approximately 50-90 GPa), extensive attempts have been made to synthesize β-C_3N_4. The first claim of the successful synthesis of β-C_3N_4, by RF sputtering of graphite in pure nitrogen onto silicon, was made in 1992 [3,4]. This claim was based on x-ray diffraction (XRD) and transmission electron diffraction. Most recent claims of successful, β-C_3N_4 growth have tried to supplement diffraction data with composition, bonding, and hardness results. For example, Gu *et al.* used microwave plasma chemical vapor deposition of CH_4 and N_2 onto Si, Pt and Ta substrates [5,6]. They claimed a mix of α and β carbon nitride based on XRD and a N/C ratio of 1.3 from energy-dispersive x-ray analysis, which is highly unreliable for low atomic masses. X-ray photoelectron spectroscopy (XPS) results were largely dominated by surface contamination and were unreliable. Hardness values of 24 GPa are low for what would be expected. Tajima *et al.* used hardness data (14 GPa) and XPS analysis (N/C=0.33 and peak shape) alone to infer the presence of β-C_3N_4 in a graphite- like matrix grown by shielded arc ion plating [7]. Chowdhury *et al.* used dc reactive sputtering at high substrate temperatures (600°-950°C) to acquire polycrystalline areas in an amorphous matrix

[8]. Electron diffraction showed strong polycrystalline rings, which could have been from β-C_3N_4. Rutherford backscattering (RBS) did eliminate the possibility of Si incorporation in the films, but could not separate the crystalline and non-crystalline phases in regards to composition. In conclusion, the evidence for successful growth of β-C_3N_4 has still proven to be inadequate in all claims to this date. There has yet to be research that can combine concrete evidence of composition, bonding, structure, and hardness properties into a definitive proof.

While creation of a harder carbon nitride phase may ultimately prove to be possible only in very small quantities, practical research has been conducted in the area of mechanical and corrosion properties of ultrathin amorphous CN_x films. Pinholes are a concern in thin films as they may act as sites for corrosion. Huang *et al.* demonstrated the diffusion of cobalt ions from the magnetic layer through pinholes in CN_x and CH_x overcoats during exposure to 80°C and 80% relative humidity for long periods of time [9]. Anoikin *et al.* exposed various carbon-based overcoats to 0.5M H_2SO_4 in a three-electrode cell apparatus [10]. Magnetron-sputtered amorphous carbon, CN_x, and CH_x, and ion-beam-deposited CH_x with thickness about 5 nm were found to show increased corrosion resistance in the order listed.

In this paper, we summarize our results from the last three years [11-14] in the following areas: relationship between mechanical properties and growth parameters of amorphous CN_x films, corrosion resistance of ultrathin CN_x films, and synthesis and characterization of CN_x/ZrN superlattice coatings with evidence of sp^3-bonded carbon formation.

II Amorphous CN_x thin films

II.1 Experimental Procedure

Thin (500 nm) and ultra-thin (1 to 6 nm) carbon nitride films were grown by single-cathode, unbalanced magnetron sputtering. Graphite targets with purity greater than 99.99% and pre- mixed sputtering gases of 3% and 5% N_2 in Ar were used. For thin CN_x deposition, the graphite target was dc-biased, and the substrates were pulsed dc-biased at up to 2 kHz with the positive voltage set at 10 percent of the absolute value in the negative cycle. Such pulsed biasing was used to prevent charging and to provide a stable plasma. Polished Si(001), super-smooth hard disks, and 80 nm permalloy-coated silicon were used as substrates. They were reverse - sputter - cleaned for 5 minutes at -500 V and 60 to 100 mTorr Ar. The substrates were not intentionally heated. However, substrate temperatures were found to increase up to 100°C due to ion bombardment. Films were characterized by *ex situ* Auger electron spectroscopy (composition), nano- indentation [15,16] and nano-scratching (mechanical properties), and atomic force microscopy (surface topography). Corrosion resistance testing was conducted by submerging the permalloy - coated silicon samples deposited with ultra - thin CN_x films in a buffered NaCl solution for 24 hours and counting the number of etch pits in a given area with an optical microscope. Film thickness was determined by cross-sectional transmission electron microscopy.

II.2 Results and discussion

Fig. 1 shows the Auger spectra of a CN_x film grown at 5 mTorr and -300 V bias before and after sputter cleaning. The oxygen contamination was easily removed with 2 minutes of Ar sputtering, leaving an N/C ratio of 0.06 to 0.08 as calculated with reported sensitivity factors [17]. This value is lower than earlier results due to the absence of a magnetic trap, which increases the ratio of ions to neutrals arriving at the substrate surface [18,19]. Fig. 2 shows only a slight dependence of N/C on the substrate bias and the total pressure. The slight drop in N/C at high bias is attributed to preferential sputtering of nitrogen.

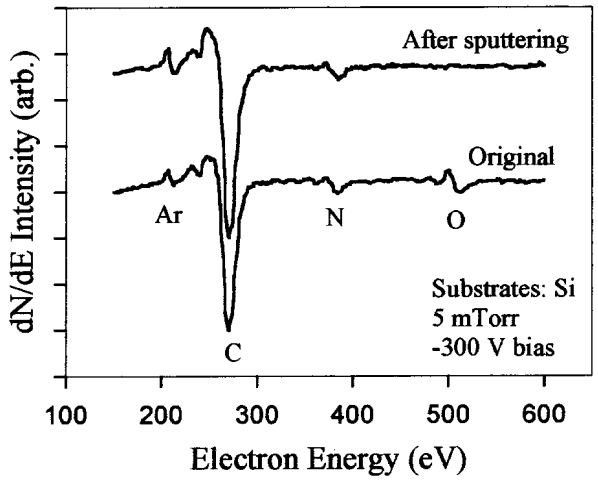

Figure 1. Auger electron spectra of a CN_x film deposited onto Si before and after sputter cleaning. Deposition pressure=5 mTorr; substrate bias=-300 V.

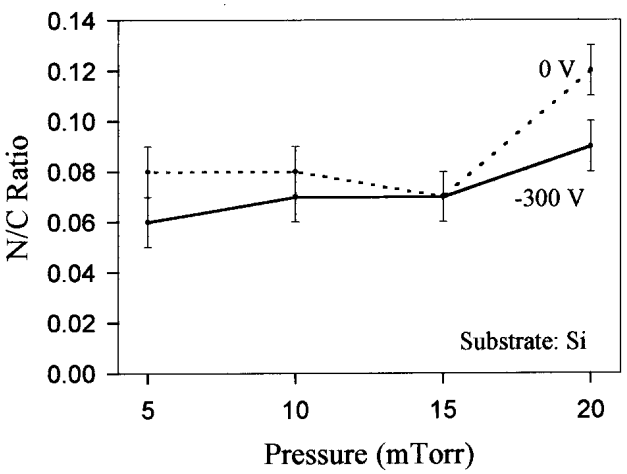

Figure 2. Influence of the total pressure on the N/C atomic ratio for films deposited on Si at zero and -300 V bias.

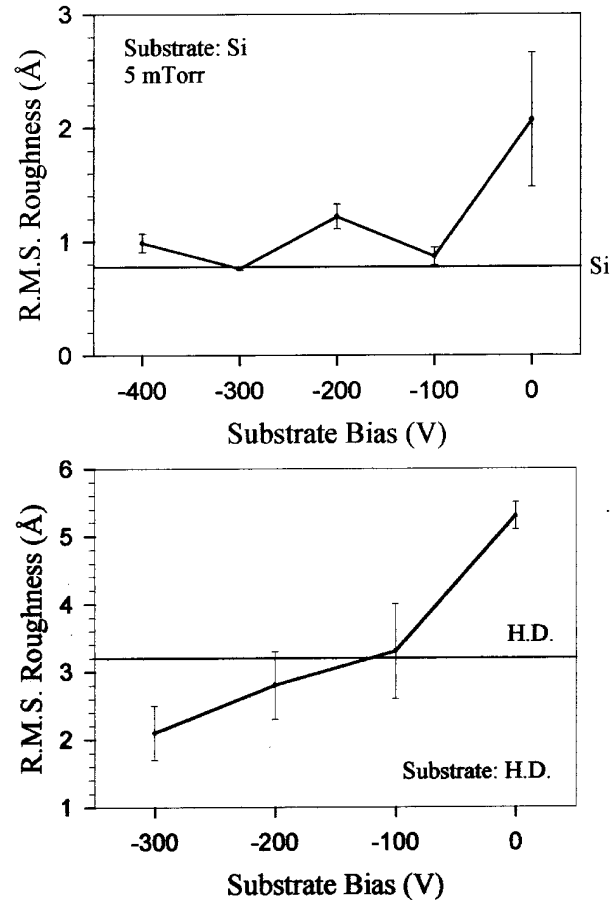

Figure 3. Variation of the rms roughness as a function of substrate bias for films deposited on (a) Si and (b) hard disk substrates. Deposition pressure =5 mTorr. Substrate roughness also shown.

Surface roughness decreases with increasing bias on both Si(001) and hard disk substrates as shown in Fig. 3. This is due to increased ion bombardment and enhanced surface diffusion of species at higher bias. Increasing the deposition pressure decreases the mean free path of positive ions in the plasma, causing them to impinge on the film with lower average energy and lower flux. At low bias, this has a significant impact on the roughness of films as seen in Fig. 4. At -300 V bias, the effect is much less pronounced. Total pressure and bias can also influence the hardness of carbon nitride films as shown in Figs. 5 and 6. Ion bombardment at an optimum energy densities films and increases the internal stress. This is seen as an increase in hardness with bias in Fig. 5. Hardness decreases with increasing gas pressure, once again due to ion bombardment at lower flux and average energy. Hardness values range from 22 to 28 GPa, which is comparable to earlier work [18,19].

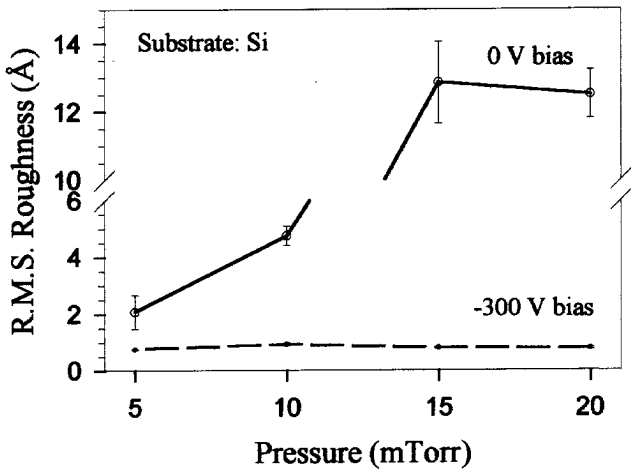

Figure 4. Variation of the rms roughness as a function of deposition pressure for films deposited on Si.

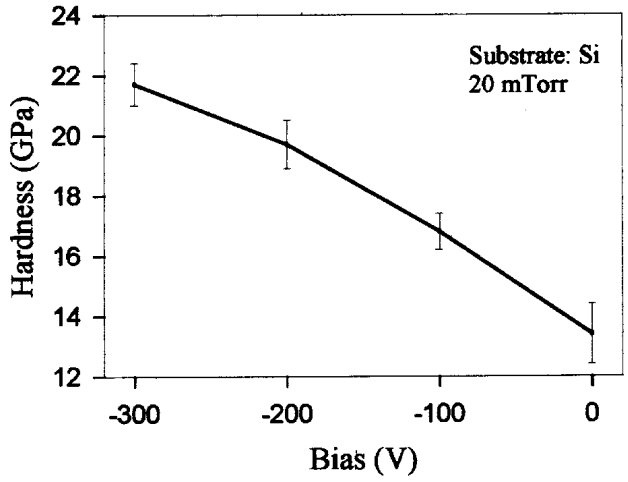

Figure 5. Influence of substrate bias on hardness of CN_x films deposited on Si. Deposition pressure=20 mTorr.

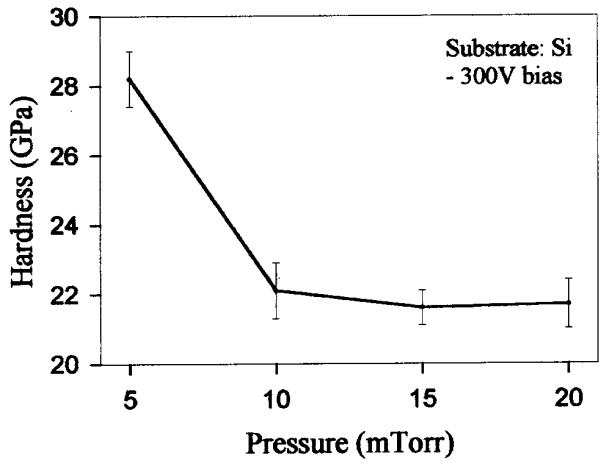

Figure 6. Influence of deposition pressure on the hardness of CN_x films deposited on Si. Substrate bias=-300 V.

Not only does bias improve hardness, it also improves the scratch resistance as seen in Fig. 7. Ultra-thin films (6 nm) grown at 0 and -200 V bias were scratched at loads from 50 to 250 μN. Films grown at -200 V bias are more scratch-resistant than those grown at zero bias (Fig. 7).

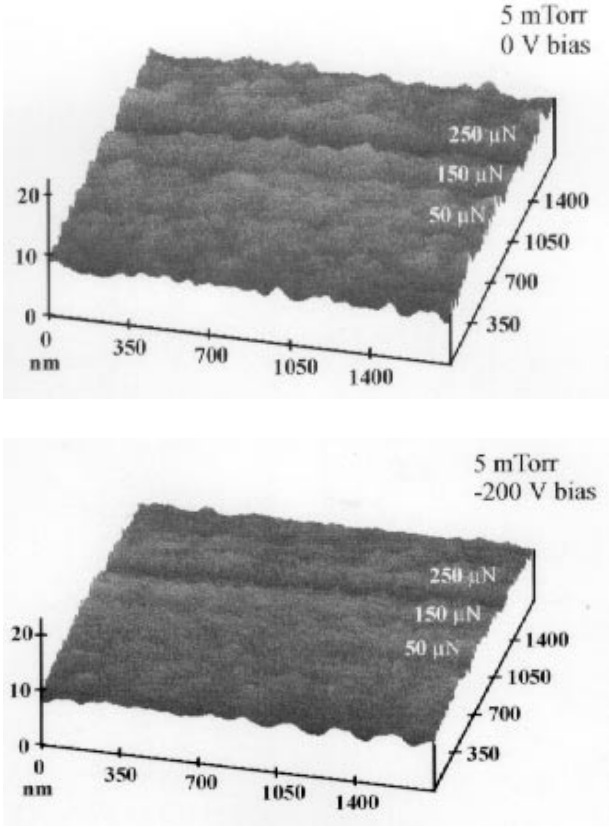

Figure 7. AFM images of scratches produced at different loads on 6 nm thick CN_x films deposited onto hard disk substrates: (a) deposited at 5 mTorr and zero substrate bias, (b) deposited at 5 mTorr and -200 V substrate bias.

Results of corrosion tests [20] on permalloy-coated Si samples deposited with different CN_x thickness are shown in Fig. 8. Substrate bias markedly improves the corrosion performance, observed as a drastic reduction in the number of corrosion pits. Acceptable industrial performance, as indicated by the dotted line, can only be achieved in films grown at zero substrate bias with thickness greater than 10 nm. At -200 V bias pulsed at 2 kHz, 1 nm thick films are acceptable!

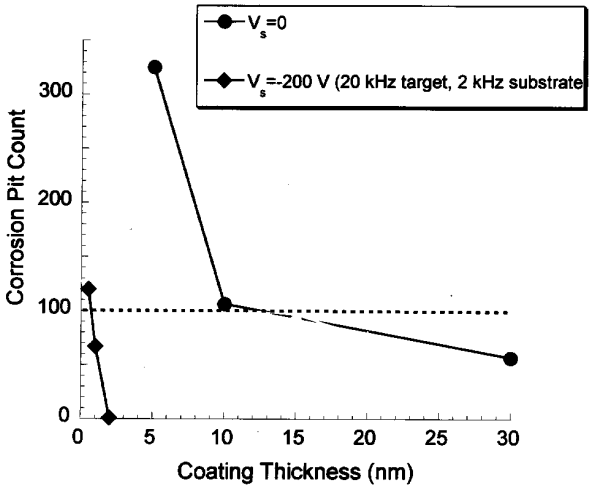

Figure 8. Corrosion resistance for ultrathin CN_x films grown at zero and -200 V substrate bias. The dashed line indicates acceptable performance.

III Crystalline CN_x/ZrN superlattice coatings

The inability to readily synthesize crystalline carbon nitride suggests that it is at best metastable. However, a structural template with symmetry and lattice size similar to that of β-C_3N_4 could be used as a stabilizing seed layer. This approach has been used to stabilize metastable cubic AlN in AlN/TiN and AlN/VN mutilayers [21,22]. Simple bilayer films have also been used. Cubic Sn, which is unstable above 13°C, was stabilized above room temperature with the use of a CdTe template [23]. CoSi with CsCl structure was stabilized on Si(111) [24].

TiN and ZrN are excellent candidates as templates for β-C_3N_4. Both have a NaCI structure and low energy (111) planes with hexagonal symmetry matching the symmetry of β-C_3N_4 (0001) planes. In addition, they have only 7% and 0.3% lattice mismatch with β-C_3N_4 on these planes, respectively. Our group reported and recently reviewed our work with CN_x/TiN superlattices, showing that there is a strong correlation between TiN texture and hardness [25-27]. Given the large elastic modulus of β-C_3N_4, even a small lattice mismatch may result in a small critical thickness

above which β-C_3N_4 becomes unstable. Therefore, we focussed our effort primarily on the local bonding state of carbon.

III.1 Experimental procedure

A dual-cathode unbalanced magnetron sputtering system was used to deposit CN_x/ZrN superlattices. Si and M1 steel substrates were mounted on a rotating holder between two opposing targets of graphite and zirconium. Total pressure (Ar and N_2) was held at 8 mTorr while the partial pressure of N_2 was varied. Target power and holder rotational speed were used to control the thickness of the CN_x and ZrN layers. The substrates were pulse dc-biased as described in the preceding section. Substrates were not intentionally heated, but did reach 200°C due to plasma heating.

Samples were hardness-tested with a UMIS ultramicroindenter and a Hysitron nanoindenter using the data analysis methods described by Oliver and Pharr [15,16]. Chemical composition was determined with Rutherford backscattering spectrometry (RBS) using a 2 MeV He^+ beam from a Van de Graff accelerator and simulated via the RUMP code [28]. XRD, high resolution transmission electron microscopy (HRTEM) and z-contrast in a scanning transmission electron microscope were used to determine the layer morphology and crystal structure. Bonding information was obtained with Raman spectroscopy and near-edge x-ray absorption fine structure spectroscopy (NEXAFS).

III.2 Results and discussion

Hardness of 46 GPa was achieved under optimized conditions of N_2 partial pressure, Zr target power, substrate bias, and rotational speed (i.e., layer thickness). In addition, hardness was found to correlate strongly with the ZrN (111) texture, supporting our hypothesis that crystalline CN_x can be stabilized with seeding layers. Fig. 9 shows that hardness and ZrN (111) texture are both maximized near 0.4 mTorr pressure of N_2.

The Zr target power has a significant effect on hardness and ZrN (111) texture as shown in Fig. 10. Increasing the Zr target power was expected to increase the proportion of ZrN in the film, leading to the conclusion that the films should become softer, not harder. However, the XRD results show that the texture of ZrN is also increased due to greater mobility of the Zr atoms, allowing them to form lower energy (111) planes: our template material. Hence, the films become harder.

Fig. 11 shows the XRD and hardness results as a function of substrate holder rotational speed. Hardness attains a maximum value at about 24 rpm (~1.4 nm bilayer thickness). Hardness decreases at the faster speeds because intermixing prevents the formation of distinct CN_x layers. At slower speeds, the CN_x layers become too thick to remain stable. Individual CN_x layer thickness must be kept below 1.0 nm to attain these high hardness values.

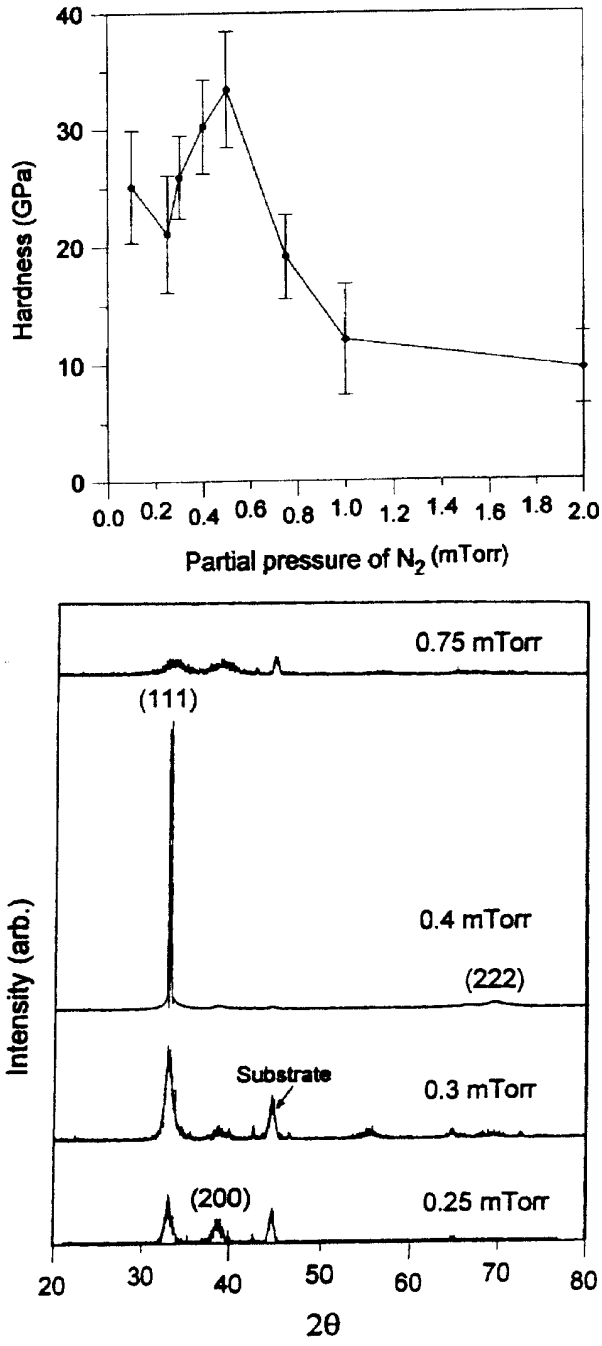

Figure 9. (a) Hardness and (b) ZrN(111) texture dependence on N2 partial pressure in CN_x/ZrN superlattice films. Zr target power=4 kW; C target power=5 kW; substrate bias=-150 V; substrate rotation=12 rpm.

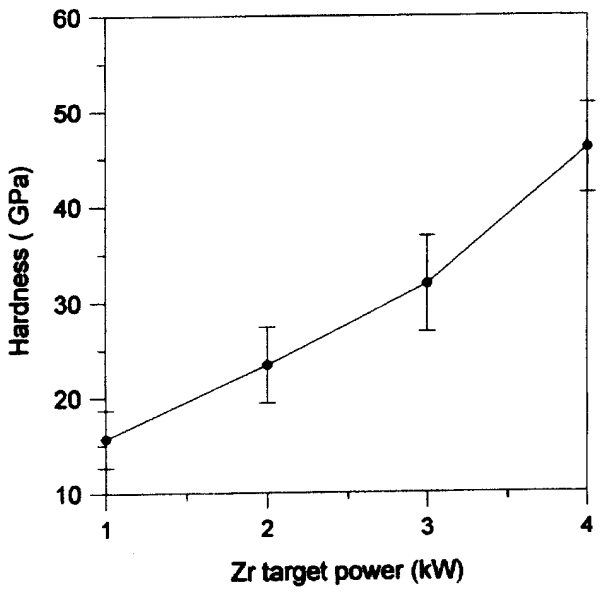

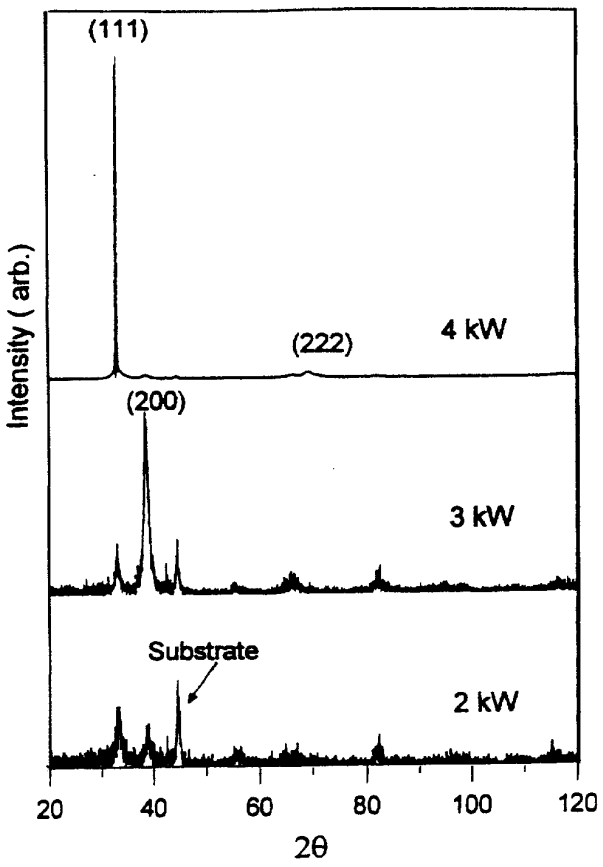

Figure 10. (a) Hardness and (b) ZrN(111) texture dependence on Zr target power in CN_x/ZrN superlattice films. C target power=5 kW; p(N_2)=0.4 mTorr; substrate bias=-150 V; substrate rotation=12 rpm.

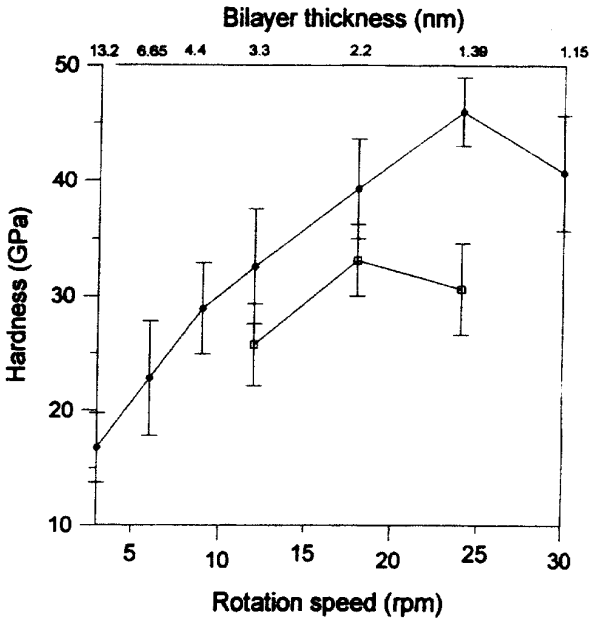

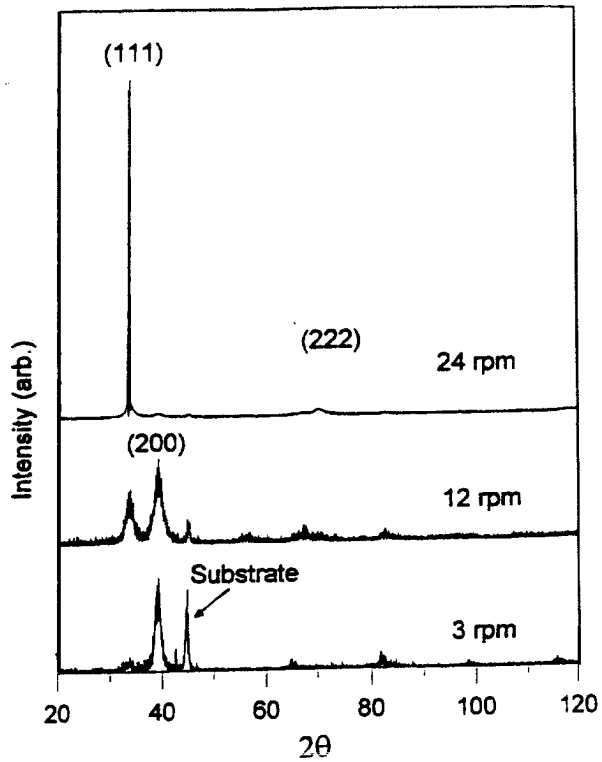

Figure 11. (a) Hardness and (b) ZrN(111) texture dependence on substrate rotational speed in CN_x/ZrN superlattice films. Zr target power=4 kW; C target power=5 kW; substrate bias=-150 V. (•) p(N_2)=0.4 mTorr; (□) p(N2)=0.3 mTorr.

While XRD gave information on texture and crystallinity of ZrN layers, it did not reveal anything about the structure of the CN_x layers. Thus, HRTEM was used. A high resolution image of a film with bilayer thickness of 7.2 nm is shown in Fig. 12. The superlattice structure is apparent with the lighter, thinner layers being the CN_x. Certain CN_x regions show lattice

fringes suggestive of crystalline growth. However, there is a possibility that these fringes are the result of ZrN island growth through the CN_x and not to crystalline CN_x itself. To disprove this possibility, z-contrast imaging was performed. A sample with bilayer thickness of 4.5 nm shows distinct layers (Fig. 13). ZrN island growth through the CN_x layers did not occur. The combination of HRTEM and z-contrast imaging suggests (but does not prove) the occurrence of crystalline CN_x growth in CN_x/ZrN superlattices.

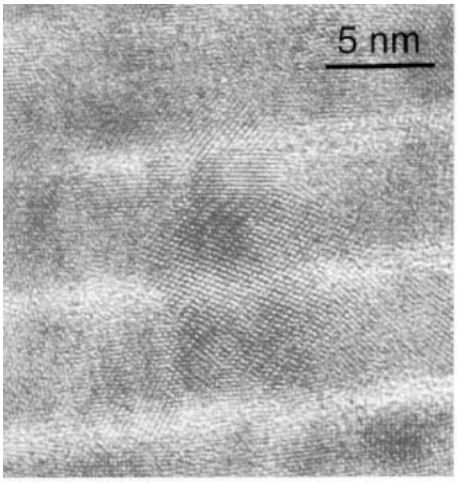

Figure 12. HRTEM image of a CN_x/ZrN superlattice thin film with bilayer thickness of 7.2 nm. The dark layers are ZrN and the light layers are CN_x.

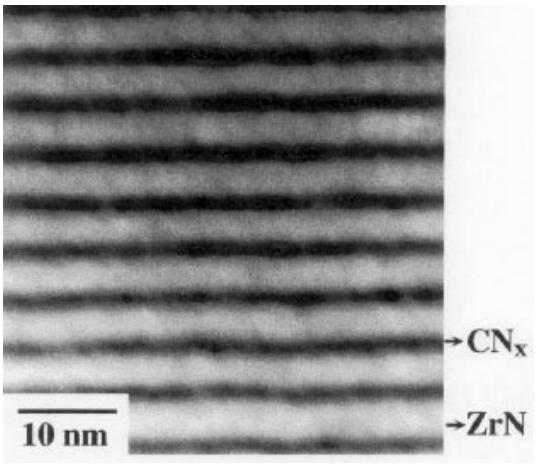

Figure 13. Z-contrast image of a CN_x/ZrN superlattice thin film with bilayer thickness of 4.5 nm. The dark layers are CN_x and the light layers are ZrN.

Composition and bonding information are also important in determining the presence of β-C_3N_4 in the films [29]. Fig. 14 shows the RBS results for a CN_x/ZrN superlattice coating with 21 bilayers with thickness of 7.2 nm (1.8 nm of CN_x and 5.4 nm of ZrN). The best fit to the data was determined to be $ZrN_{0.5}$ and $CN_{1.3}$, assuming the density of the carbon nitride to be 1.6×10^{23} atoms/cm^3 (cf. theoretical value of 1.64×10^{23} atoms/cm^3). Cross-sectional Raman spectroscopy shows a transition from sp^2 to sp^3 bonding for carbon atoms when the bilayer thickness decreases from 10.3 nm to 1.6 nm (Fig. 15). The spectrum for 1.6 nm does not exhibit the characteristic D, G, and out-of-plane bending mode bands of sp^2 carbon at 1350, 1550, and 680 cm^{-1}, respectively. In addition, a peak near 600 cm^{-1}, which could be attributed to β-C_3N_4, appears [30].

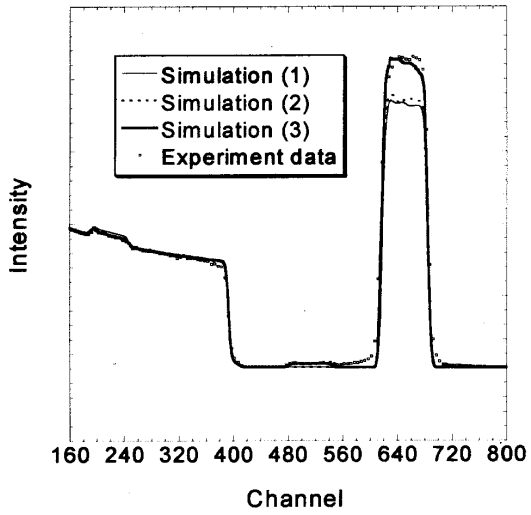

Figure 14. RBS spectrum of a CN_x/ZrN superlattice thin film with bilayer thickness of 7.2 nm, along with various simulation fits based on the density. Simulation (1): ZrN (8.382×10^{22} atoms/cm^3) and CN (1.45×10^{23} atoms/cm^3); simulation (2): ZrN (8.382×10^{22} atoms/cm^3) and C (1.6×10^{23} atoms/cm^3); simulation (3): $ZrN_{0.5}$ (6.8×10^{22} atoms/cm^3) and C_3N_4 (1.6×10^{23} atoms/cm^3) and 0.5 at. % of Ar.

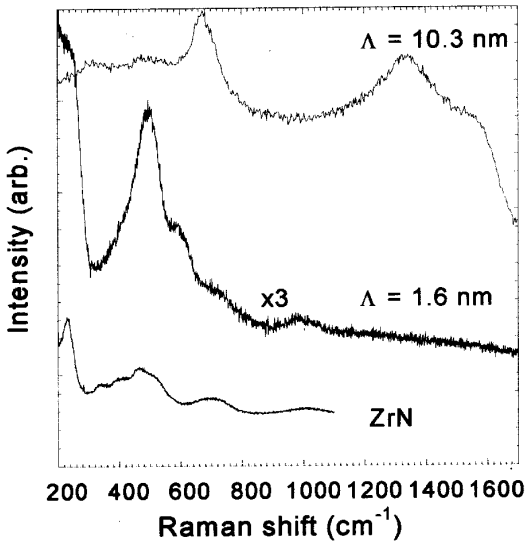

Figure 15. Raman spectra from a pure ZrN thin film and CN_x/ZrN superlattices with different periods.

The NEXAFS results also show the disappearance of sp/sp^2 carbon as the bilayer thickness decreases (Fig. 16). The π^* peak at 285 eV, which is clearly visible in amorphous CN_x, is absent in the CN_x/ZrN superlattices with bilayer thickness of 4.5 nm or less. These results indicate the presence of sp3-bonded carbon atoms in the CN_x/ZrN superlattice coatings.

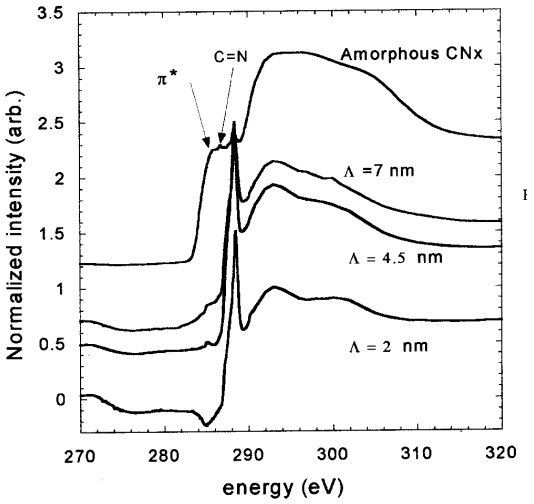

Figure 16. Carbon K-edge NEXAFS spectra from an amorphous CN_x thin film and CN_x/ZrN superlattices with different periods.

IV Summary

Amorphous carbon nitride (CN_x) and CN_x/ZrN superlattice coatings were deposited by reactive magnetron sputtering. Film hardness and texture was related to growth parameters such as substrate bias, target power, and gas pressure. Ultrathin (1 nm) CN_x films, when prepared under optimum conditions, can provide adequate corrosion protection for hard disk applications. There is a strong correlation between ZrN (111) texture and hardness in CN_x/ZrN superlattice coatings. Raman spectroscopy and NEXAFS show the predominance of sp3-bonded carbon in these superlattice coatings.

Acknowledgments

The authors wish to acknowledge the NSF Surface Engineering and Tribology program (grant No. CMS-9610440), the NSF MRSEC program (grant No. DMR-9632472) and NSIC for support of this work. Results summarized in this review were made possible by the dedicated work of Louis Chan, Murat Guruz, Mei-Ling Wu, and Dr. Ben Zhou. We are thankful for the discussions with Profs. V. D. Dravid, L. D. Marks, W. D. Sproul and Dr. W.-A. Chiou and collaboration with Profs. F.L. Freire, Jr., G. Mariotto and Drs. S. Anders and C. S. Bhatia. Thanks are also due to Nissei Sangyo America, Ltd. (Mr. McIlwrath and Mr. Gordon) for access to HD-2000 STEM.

References

[1] A.Y. Liu, and M. L. Cohen, Science, **245**, 841 (1989).

[2] A.Y. Liu, and M. L. Cohen, Physical Review B, **41**, 10727 (1990).

[3] E.E. Haller, and M. L. Cohen, USPatent, 5, 110, 679, May 5, 1992

[4] Yu, K. M., M. L. Cohen, E. E. Haller, W. L. Hansen, A. Y. Liu, and I. C. Wu, Physical Review B, **49**, 5034 (1994).

[5] Y.S. Gu, Y. P. Zhang, Z. J. Duan, X. R. Chang, Z. Z. Tian, N. X. Chen, C. Dong, D. X. Shi, X. F. Zhang, and L. Yuan, Journal of Materials Science, **34**, 3117 (1999).

[6] Y.S. Gu, Y.P. Zhang, Z.J. Duan, X.R. Chang, Z.Z. Tian, D.X. Shi, L.P. Ma, X.F. Zhang, and L. Yuan, Materials Science and Engineering, A **271**, 206 (1999).

[7] N. Tajima, H. Saze, H. Sugimura, and 0. Takai, Japanese Journal of Physics **2**, 38, 10A, L1131 (1999).

[8] A.K.M.S. Chowdhury, D.C. Cameron, M.S.J. Hashmi, and J. M. Gregg, Journal of Materials Research, **14**, 6 2359 (1999).

[9] L.J. Huang, Y. Hung, and S. Chang, IEEE Transactions on Magnetics, **33**, 3154 (1997).

[10] E.V. Anoikin, G.S. Ng, M.M. Yang, J.L. Chou, J.R. Elings, and D.W. Brown, IEEE Transactions on Magnetics, **34**, 1717 (1998).

[11] W.C. Chan, B. Zhou, Y. W. Chung, C. S. Lee, and T. S. Lee, Journal of Vacuum Science and Technology A **16**, 1907 (1998).

[12] M.L. Wu, X.W. Lin, V. P. Dravid, Y.W. Chung, M.S. Wong, and W.D. Sproul, Journal of Vacuum Science and Technology A **15**, 946 (1997).

[13] M.L. Wu, W.D. Qian, Y.W. Chung, Y.Y. Wang, M. S. Wong, and W. D. Sproul, Thin Solid Films, **308-309**, 113 (1997).

[14] M.L. Wu, Z. Yang, Y.W. Chung, M.S. Wong, and W. D. Sproul, Journal of Tribology, **120**, 179 (1998).

[15] W.C. Oliver, and G. M. Pharr, Journal of Materials Research, **7**, 1564 (1992).

[16] G.M. Pharr, and W.C. Oliver, MRS Bulletin, **17**, 28 (1992).

[17] L.E. Davis, N.C. MacDonald, P.W. Palmberg, G.E. Rial, and R.E. Weber, *Handbook of Auger Electron Spectroscopy,* (Perkin-Elmer, Physical Electronics Industries, Eden Prairie, MN, 1978).

[18] E.C. Cutiongco, D. Li, Y.W. Chung, and C.S. Bhatia, Journal of Tribology, **118**, 543 (1996).

[19] Y. Marumo, Z. Yang, and Y.W. Chung, Surface and Coatings Technology, **86/87**, 586 (1996).

[20] M.U. Guruz, Y.H. Yu, V.P. Dravid, Y.W. Chung, M. Lacerda and C.S. Bhatia, *Proceedings of the Symposium on Interface Technology: Towards 100 Gbit/in^2*, 47 (1999).

[21] A. Madan, I.W. Kim, S.C. Cheng, P. Yashar, V.P. Dravid, and S.A. Barnett, Physical Review Letters, **79**, 1743 (1997).

[22] Q. Li, S.A. Barnett, and L. Marks, Scanning, **21**, 158 (1999).

[23] T.S. Lin, W.J. Partin, and Y.W. Chung, *Materials Research Society Symposium Proceedings,* **77**, 247, edited by J.P. Dow and I.K. Schuller, Pittsburgh (1987).

[24] H. von Känel, C. Schwarz, S. Gonclaves-Conto, E. Müller, L. Miglio, F. Tavazza, and G. Malegori, Physical Review Letters, **74**, 1163 (1995).

[25] D. Li, X. Chu, S.C. Cheng, X.W. Lin, Y.W. Chung, V.P. Dravid, M.S. Wong, and W.D. Sproul, Applied Physics Letters, **67**, 203 (1995).

[26] D. Li, X.W. Lin, S.C. Cheng, Y.W. Chung, and V.P. Dravid, Applied Physics Letters, **68**, 1211 (1996).

[27] B. Zhou, and Y.W. Chung, Journal of the Chinese Institute of Engineers, **21**, 691 (1998).

[28] L.R. Doolitle, Nuclear Instruments and Methods in Physics Research B **9**, 344 (1985).

[29] M.L. Wu, PhD thesis, Northwestern University (1999).

[30] T.Y. Yen, and C.P. Chou, Applied Physics Letters, **67**, 2801 (1995).